Received: 27 June 2022 | Revised: 2 September 2022 | Accepted: 27 September 2022

IET Microwaves, Antennas & Propagation

DOI: 10.1049/mia2.12305

ORIGINAL RESEARCH

High-gain wideband circularly polarised mm-wave antenna with highly symmetrical radiation patterns

Xianting Xie[1] | Long Zhang[1] | Chunxu Mao[2] | Yejun He[1] | Steven Gao[3]

[1]College of Electronics and Information Engineering, Shenzhen University, Shenzhen, China

[2]Institute for Communication Systems (ICS), 5G Innovation Centre (5GIC), University of Surrey, Guildford, UK

[3]Department of Electronic Engineering, The Chinese University of Hong Kong, Hong Kong, China

Correspondence

Long Zhang, College of Electronics and Information Engineering, Shenzhen University, Shenzhen 518060, China.
Email: long.zhang@szu.edu.cn

Funding information

Natural Science Foundation of Guangdong Province, Grant/Award Number: 2020A1515011037; National Natural Science Foundation of China, Grant/Award Numbers: 61801299, 62071306; Shenzhen Science and Technology Program, Grant/Award Numbers: JCYJ20200109113601723, JSGG20210420091805014, JSGG20210802154203011

Abstract

A circularly polarised (CP) antenna with highly symmetrical radiation patterns and wide operating bandwidth is presented for millimetre-wave (mm-wave) applications. By loading four parasitic inverted-F components around a SIW-fed S-dipole antenna, better axial ratio (AR) performance and higher gain performance are realised. Furthermore, the proposed antenna can achieve highly symmetrical radiation patterns in different elevation planes within a wide operating band. This unique feature makes it advantageous to more uniform signal coverage. To verify the effectiveness of the antenna, a prototype is fabricated and measured. The experimental results validate that the antenna covers the impedance bandwidth of 49.1% (21.2–35 GHz) and the AR bandwidth of 51.3% (20–33.8 GHz). Besides, the antenna peak gain can reach 10.42 dBic at 28.5 GHz. More importantly, the antenna can radiate extremely symmetrical and uniform waves in different elevation planes within a wide operating band (21–29 GHz). Attributed to these merits, the presented antenna shows great potential in various mm-wave systems.

KEYWORDS

circularly polarised antenna, millimetre-wave antenna, substrate integrated waveguide, wideband antenna

1 | INTRODUCTION

With the rapid rise of emerging wireless systems, higher requirements are put forward for high-speed data transmission. Compared with the sub-6 GHz band, the spectrum resources at millimetre-wave (mm-wave) bands are more abundant, which drives the research and development of low-cost wideband mm-wave antennas [1, 2]. Due to the effectiveness in mitigating multipath interference and fading, the circularly polarised (CP) antennas have aroused great interest in wireless communication systems [3, 4]. For these reasons, wideband mm-wave CP antennas attract increasing interests in recent years.

Considering that the dielectric loss and radiation loss are no longer negligible at mm-wave frequencies, the substrate integrated waveguide (SIW) is thus extensively deployed in designing mm-wave antennas due to its low loss, easy integration, and high power handling capability characteristics [5, 6]. To date, a variety of mm-wave wideband SIW CP antennas were proposed, including the horn antennas [7–9], dielectric resonator antennas (DRA) [10–12], slot antennas [13–17], magneto-electric dipole antennas [18, 19], parasitic patches loaded antenna [20], patch antennas [21–23], L-probe antenna [24], and spiral antenna [5, 25]. In ref. [7], an SIW horn antenna loaded with an inhomogeneous polariser was presented. The wide impedance bandwidth is obtained by introducing an extended substrate and additional dielectric plates around the horn radiation aperture, and the broadband CP radiation is realised by applying a pure dielectric polariser. However, it's broadband characteristic of the antenna is achieved at the expense of high antenna profile. In ref. [10], a wideband CP substrate integrated DRA was introduced. The basic mode of the internal dielectric resonator and the higher

order mode of the whole dielectric resonator can be excited simultaneously at adjacent frequencies, thus improving the impedance and axial ratio (AR) bandwidth. In ref. [19], the bowtie dipole and isosceles triangular grooves were utilised to realise better CP performance of the antenna.

Although the aforementioned antennas have broad bandwidth, most of these studies pay little attention to the symmetry and stability of the radiation patterns. Maintaining symmetrical and stable radiation patterns is extremely challenging and appealing to various applications, such as the positioning systems, the cognitive radio application [26], phased arrays [27] and base stations [28]. To this end, this paper aims to design a wideband mm-wave CP antenna with stable and symmetrical radiation patterns.

In this paper, a parasitic inverted-F components (PIFCs) loaded SIW S-dipole antenna with both broadband and high-gain merits is proposed for mm-wave applications. Although the SIW-fed S-dipole antenna has been proposed in ref. [1], there are several drawbacks for this antenna. Firstly, the AR bandwidth is narrower than its impedance bandwidth, leading to a reduced operating bandwidth. In addition, the peak gain is just 7.5 dBic, which needs to be improved to combat with the free-space loss at mm-wave bands. Most importantly, the radiation pattern of this antenna is quite asymmetrical in different elevation planes, which limits its applications. To solve these issues, four PIFCs are placed sequentially rotated around the SIW-fed S-dipole. As four PIFCs are loaded, the aperture size of the antenna is increased, thus effectively improving the antenna gain. Moreover, another new AR resonance occurs with the presence of the PIFCs, which broadens the AR bandwidth and the overall bandwidth. Furthermore, the coupling between the S-dipole and PIFCs helps maintain more uniform and stable E-fields distribution in different elevation planes. As a consequence, a highly symmetrical radiation pattern in different elevation planes can be obtained, which is verified by the simulation and experiment results. On the whole, the merits above makes the presented antenna very competitive in applications where a highly symmetrical radiation pattern is required.

2 | ANTENNA DESIGN AND OPERATING PRINCIPLE

2.1 | Antenna design

Figure 1 demonstrates the configuration of the proposed antenna. As shown, an S-dipole is printed on the top surface of substrate 1, which is surrounded by four PIFCs. The electromagnetic coupling between the SIW and the S-dipole is realised by the coupling slot. By adjusting the width and length of the slot, the antenna performance can be effectively improved. A coaxial probe is applied to feed the antenna directly, and it also helps obtain good impedance matching. Detailed geometry parameters of the antenna is listed in Table 1.

Figure 2 shows the magnitude of surface current on the antenna at three different resonant frequencies, indicating that the antenna operates in a quasi-0.75λ, quasi-1λ and quasi-1.25λ mode at these three frequencies respectively. In this manner, the proposed antenna can operate over a wide bandwidth. Moreover, the stable and symmetrical radiation is obtained by the coupling between the S-dipole and PIFCs.

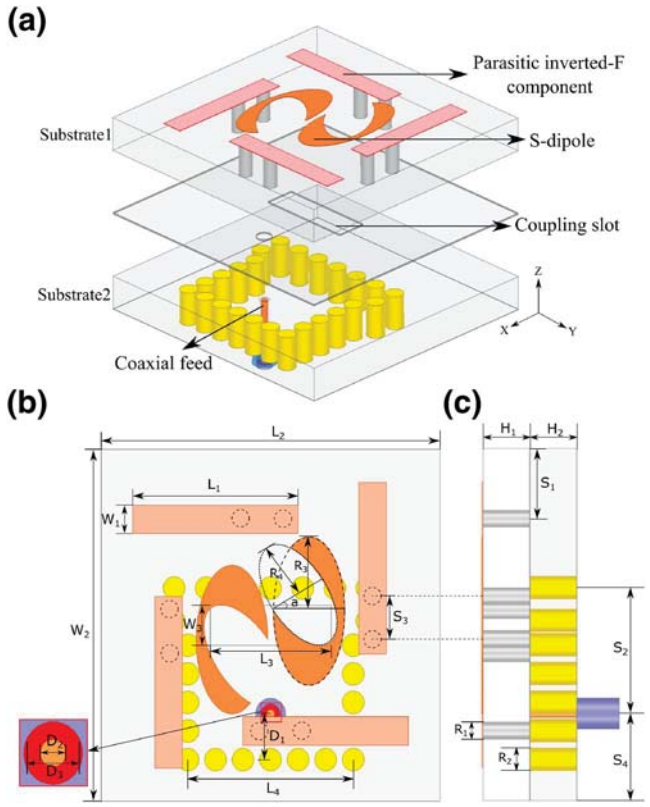

FIGURE 1 Configuration of the proposed antenna. (a) Exploded view, (b) top view and (c) side view.

TABLE 1 Antenna parameters (unit: mm)

L_1	L_2	L_3	L_4	W_1	W_2	W_3	D_1	D_2	D_3
6	12.3	4.4	6	1	12.3	1.4	1.6	0.3	0.7
R_1	R_2	R_3	R_4	H_1	H_2	S_1	S_2	S_3	S_4
0.6	0.8	2.6	2.08	1.57	1.57	2.45	4.4	1.5	3

It is worth mentioning that the simulation software used in this paper is HFSS 2020 and the adaptive mesh property is adopted.

2.2 | Operating principle and parametric study

The CP operating principle of the SIW-fed S-dipole can be found in ref. [1], and thus is not explained here for brevity. One drawback of the SIW-fed S-dipole antenna is the narrower AR bandwidth compared to its impedance bandwidth, and the relatively low antenna gain. Another big issue for this antenna is that the radiation pattern is quite asymmetrical in two diagonal planes, leading to much different beamwidth in different elevation planes. It is worth mentioning that an

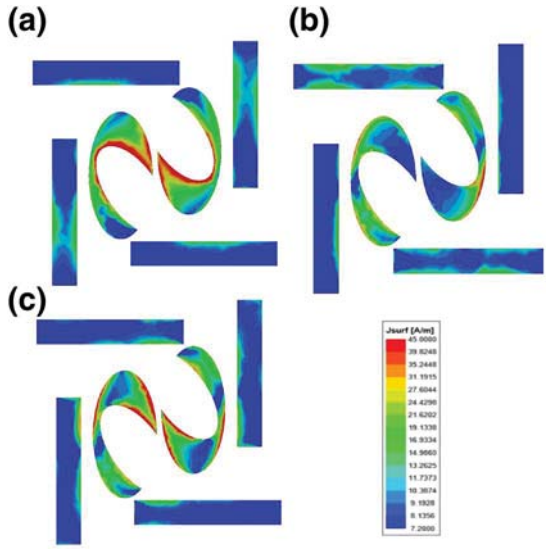

FIGURE 2 Magnitude of surface current on the S-dipole and PIFCs. (a) 23.25 GHz, (b) 26.75 GHz, and (c) 32 GHz. PIFCs, parasitic inverted-F components

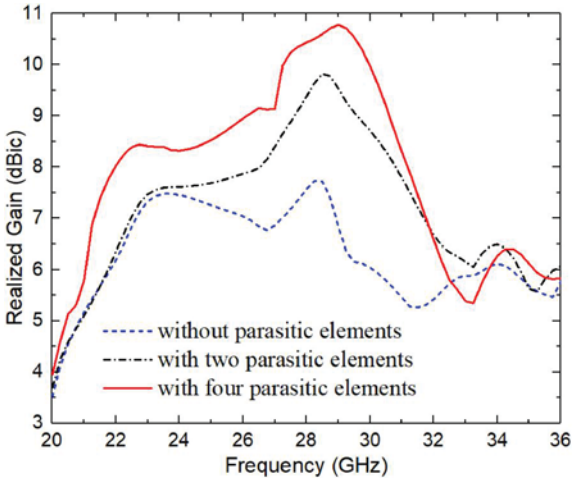

FIGURE 3 Effect of the PIFCs on the antenna gain. PIFCs, parasitic inverted-F components

antenna loaded with two parasitic components has been presented in ref. [29]. The difference between the antenna proposed in this paper and the antenna in ref. [29] mainly lies in the simplification of feeding method and the improvement of performance. Although the antenna loaded with two parasitic components improves the AR bandwidth and gain of the S-dipole antenna, it also causes the distortion of radiation pattern and excessive fluctuation of the gain curve. To solve these issues, four PIFCs are positioned sequentially rotated around the SIW-fed S-dipole, as depicted by Figure 1. With the presence of the four PIFCs, the radiation aperture becomes larger than that with two PIFCs, so the gain is higher, and the gain curve becomes more stable and smooth. Moreover, the coupling between the four PIFCs and the S-dipole makes the electric field distribution more uniform, forming a more stable and symmetrical radiation patterns in different elevation planes, which cannot be achieved with two PIFCs. In addition, the antenna is fed by a coaxial probe directly without any matching post, which simplifies the feeding structure compared to the antenna in ref. [29]. Moreover, the AR bandwidth of the proposed antenna is further improved due to the additional AR resonance introduced by the four PIFCs.

It is worth pointing out that the initial reason for using sequentially rotated parasitic components is to expand the antenna bandwidth, as demonstrated in ref. [20]. However, it is found that more uniform electric field distribution is formed by loading four PIFCs, thus generating symmetrical and stable radiation in different elevation planes. Moreover, the bandwidth and antenna gain are also improved by loading four PIFCs. In order to interpret the function of the PIFCs, the antenna performances with different geometry dimensions are studied and discussed in detail subsequently, which provides necessary explanation of the antenna operating principle.

Figure 3 examines the effect of the PIFCs on the antenna gain. As is shown in Figure 3, the gain increases as the number of PIFCs increases throughout the operating frequency band, which indicates that the gain improvement of the antenna by using PIFCs is effective. The gain improvement is mainly due to the enlarged radiation aperture of the antenna by applying the PIFCs around the S-dipole.

As the four PIFCs are sequentially rotated around the S-dipole, the coupling fields on the PIFCs can also realise CP radiation. By appropriately choosing the distance between the S-dipole and the PIFCs, the coupling fields radiate as CP waves at another frequency, which contribute to the AR bandwidth improvement. Figure 4 shows the AR comparison between the proposed antenna and the antenna without PIFCs. For a fair comparison, the parameters of the antenna without PIFCs are also optimised to obtain a good AR performance. As shown in Figure 4, the four PIFCs help improve the AR performance by introducing a new AR resonance at 23.25 GHz and reducing the AR value of another AR resonance at 32 GHz. The improvement of the AR performance is mainly attributed to the additional AR resonance introduced by the PIFCs and the fields coupling between the S-dipole and PIFCs. Figure 5 shows the influence of the distance between the S-dipole and the PIFCs (D_s) on the AR and the reflection coefficient of the proposed antenna. As shown in Figure 5, the parameter D_s plays an essential role in the AR improvement of the antenna. In addition, D_s has little effect on the reflection coefficient and gain of the antenna. As can be seen from Figures 6 and 7, the length (L_1) and width (W_1) of the PIFCs also affect the antenna's AR performance but do not impact the impedance matching.

Therefore, in the design process of the proposed antenna, D_s, L_1, and W_1 can be reasonably selected to improve the antenna AR bandwidth, and these parameters will not have a great impact on the $|S_{11}|$ and gain of the antenna. To achieve a maximum overlap between the antenna's AR and impedance bandwidth, D_s, W_1, L_1 are selected as 3.7, 1 and 6 mm respectively. Besides, the design of the S-dipole antenna could refer to [1], but its dimensions also need to be optimised due to the presence of four PIFCs. Figures 8 and 9 shows the effect

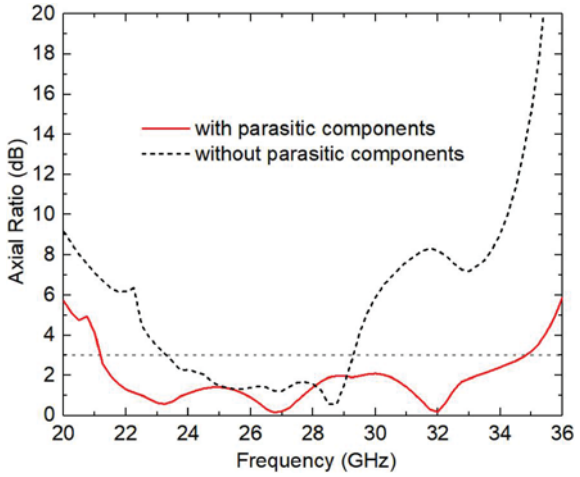

FIGURE 4 Effect of the PIFCs on the antenna AR. AR, axial ratio; PIFCs, parasitic inverted-F components

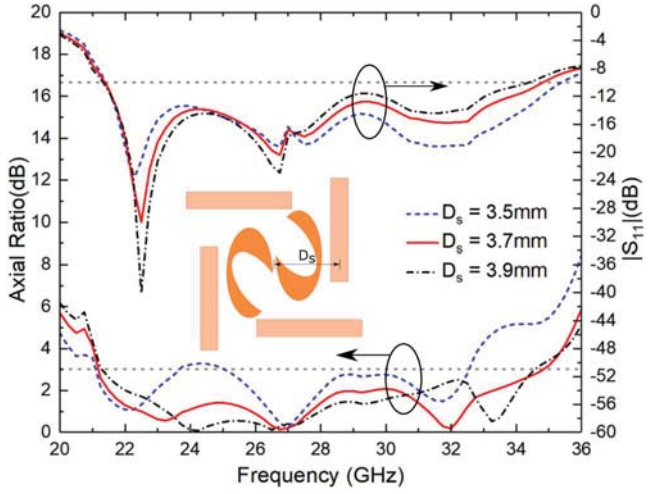

FIGURE 5 Effect of the distance between the S-dipole and the PIFCs on the AR and the reflection coefficient of the proposed antenna. AR, axial ratio; PIFCs, parasitic inverted-F components

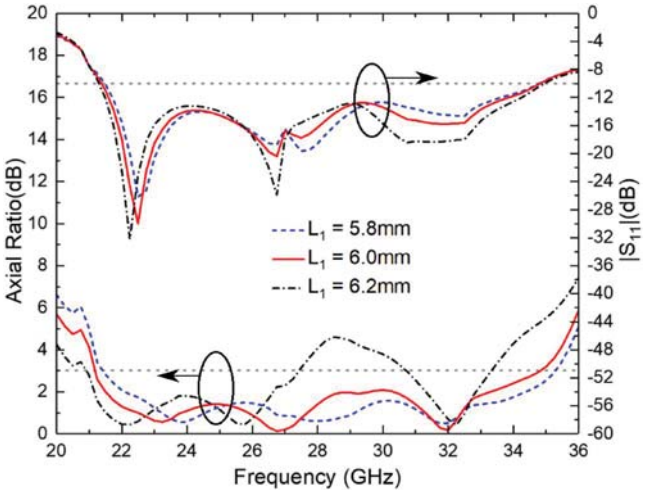

FIGURE 6 Effect of the length of the PIFC on the AR and the reflection coefficient of the proposed antenna. AR, axial ratio; PIFC, parasitic inverted-F component

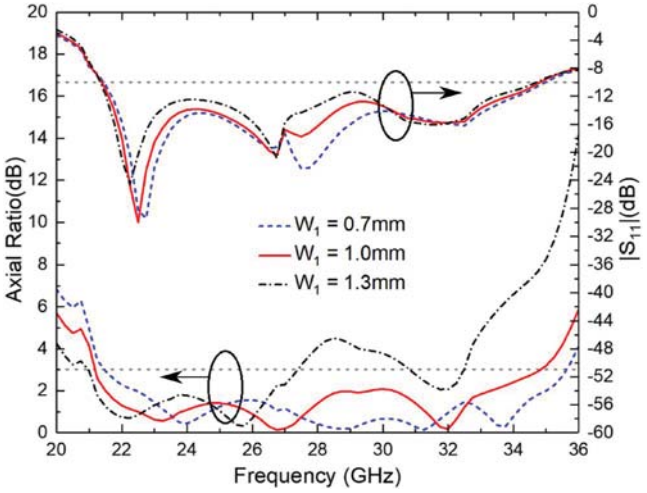

FIGURE 7 Effect of the width of the PIFC on the AR and the reflection coefficient of the proposed antenna. AR, axial ratio; PIFC, parasitic inverted-F component

of the radius (R_3) and rotation angle (α) of the S-dipole respectively. To ensure the antenna to achieve better CP performance with good impedance matching, R_3 and α are selected to be 2.6 mm and 35°, simultaneously. Figure 10 shows the influence of the coaxial probe position (D_1) on the reflection coefficient of the proposed antenna. As can be seen from Figure 10, a good impedance matching can be achieved when D_1 equals to 1.6 mm.

Figure 11 shows the E-fields distribution of the proposed antenna and the antenna without the PIFCs in four different elevation planes at 26 GHz. The dashed boxes A–D contain the PIFCs, while the boxes A′–D′ indicate the corresponding area of the antenna without PIFCs. It can be observed from Figure 11 that the proposed antenna exhibits more uniform and stable E-fields distribution in different elevation planes than that of the antenna without four PIFCs. Especially notice from Figure 11a,e that the radiation area of the antenna is increased with the existence of the four PIFCs, which compensates for non-identical radiation area in different elevation planes. Similarly, observing from the regions B and D in Figure 11b,d, the coupling fields between the PIFCs and the S-dipole also contributes to the increased radiation aperture. In this manner, the proposed antenna can maintain similar radiation area in different elevation planes, resulting in a highly symmetric radiation pattern in different elevation planes.

Figure 12 demonstrates the simulated radiation patterns of the antenna with and without PIFCs at 26 GHz. As revealed by the figure, the radiation patterns of the antenna without PIFCs are rather asymmetrical in different elevation planes. On the contrary, the radiation patterns of the proposed antenna maintain good symmetry and stability in different elevation planes. In conclusion, by loading four PIFCs, the antenna can not only achieve higher gain and wider AR bandwidth, but also ensure

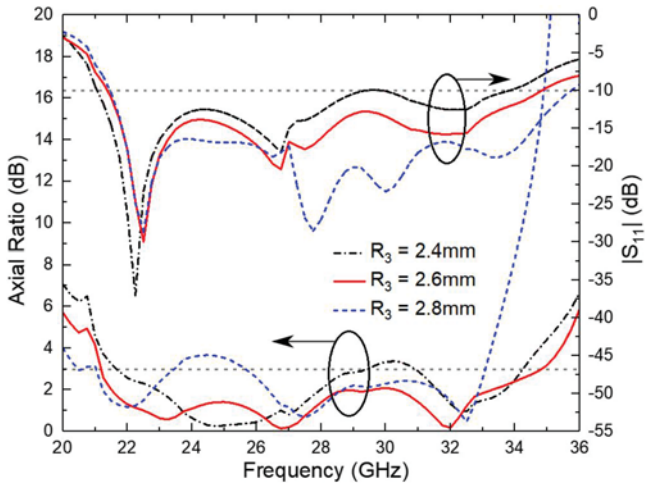

FIGURE 8 Effect of the radius of the S-dipole (R_3) on the AR and the reflection coefficient of the proposed antenna. AR, axial ratio

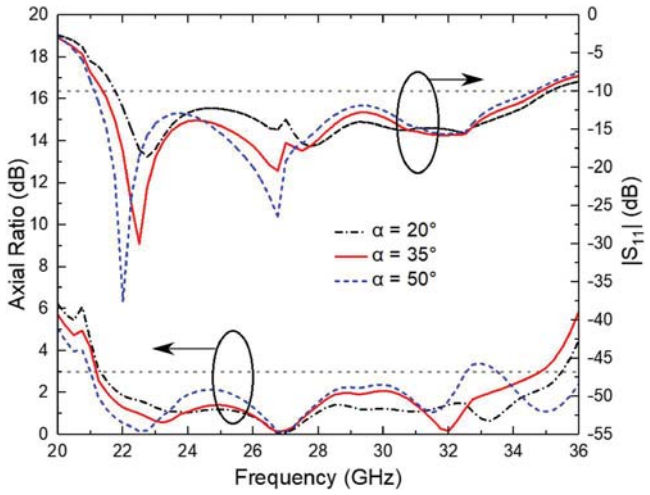

FIGURE 9 Effect of the rotation angle of the S-dipole (α) on the AR and the reflection coefficient of the proposed antenna. AR, axial ratio

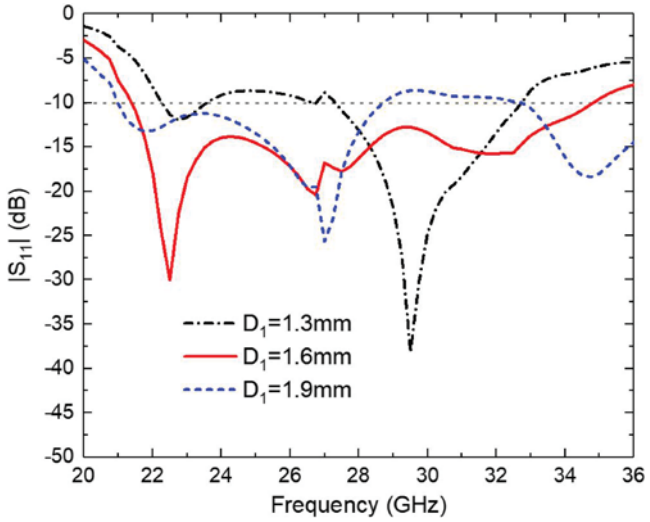

FIGURE 10 Effect of the position of the coaxial probe (D_1) on the reflection coefficient of the proposed antenna.

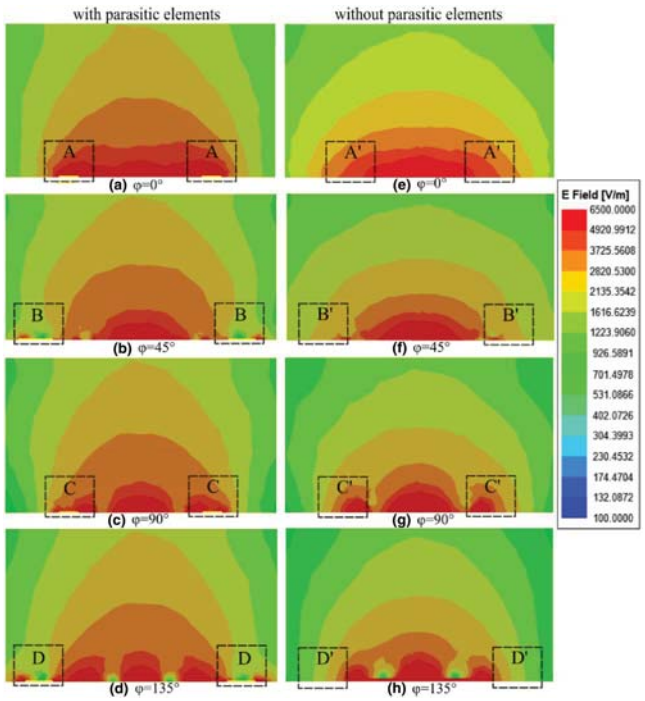

FIGURE 11 E-fields distribution of the antenna with and without PIFCs in four elevation planes at 26 GHz. (a–d) The antenna with PIFCs and (e–h) the antenna without PIFCs. PIFCs, parasitic inverted-F components

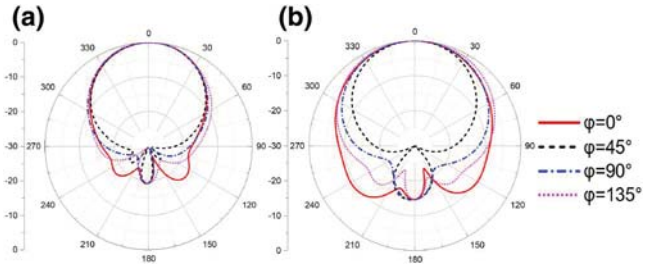

FIGURE 12 Simulated normalised RHCP radiation patterns of the antenna with and without the PIFCs respectively at 26 GHz (a) antenna with PIFCs and (b) antenna without PIFCs. PIFCs, parasitic inverted-F components; RHCP, right-handed circularly polarised

high symmetry and stability of radiation patterns in different elevation planes, so as to realise more uniform signal coverage.

Figure 13 displays the simulated normalised radiation patterns of the proposed antenna at four different frequency points. It is clear that the antenna radiates right-handed circularly polarised waves and its radiation patterns are highly symmetrical in different elevation planes over a wide frequency band, which verifies that the proposed method did work in realising symmetrical radiation patterns by using loaded components.

3 | RESULTS AND DISCUSSION

As shown in Figure 14, an antenna prototype is fabricated and measured to validate the design concept. In the prototype, the S-dipole and four PIFCs are etched on the top surface of a

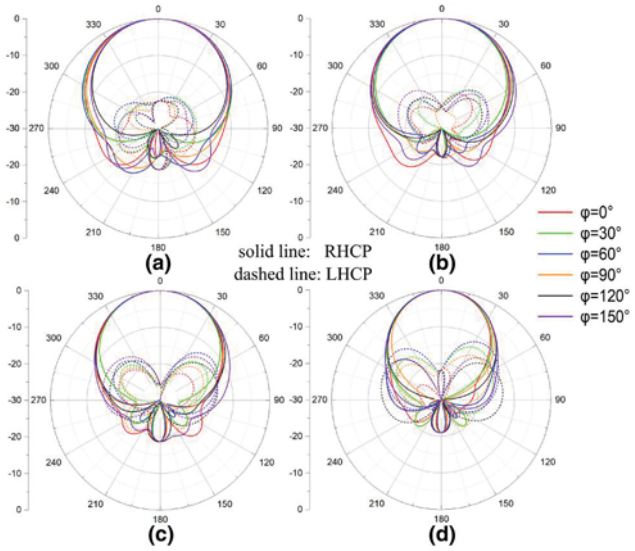

FIGURE 13 Simulated normalised radiation patterns of the proposed antenna at four different frequency points. (a) 22 GHz, (b) 24 GHz, (c) 26 GHz, and (d) 28 GHz

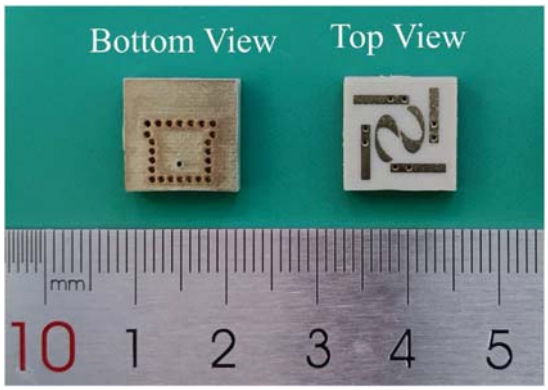

FIGURE 14 The prototype of the proposed antenna.

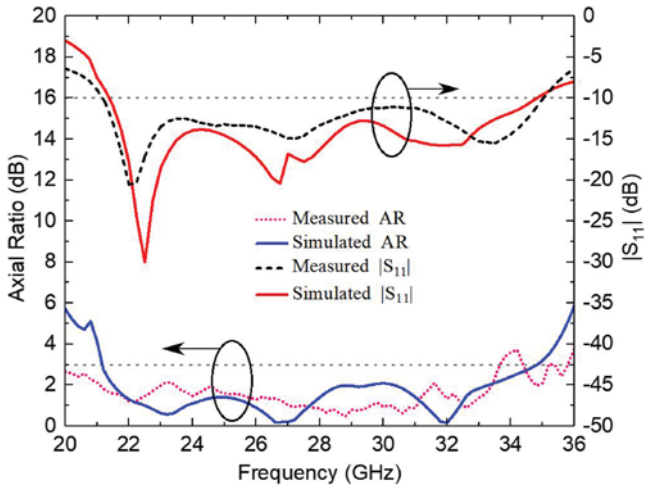

FIGURE 15 Simulated and measured reflection coefficients and ARs of the proposed antenna. AR, axial ratios

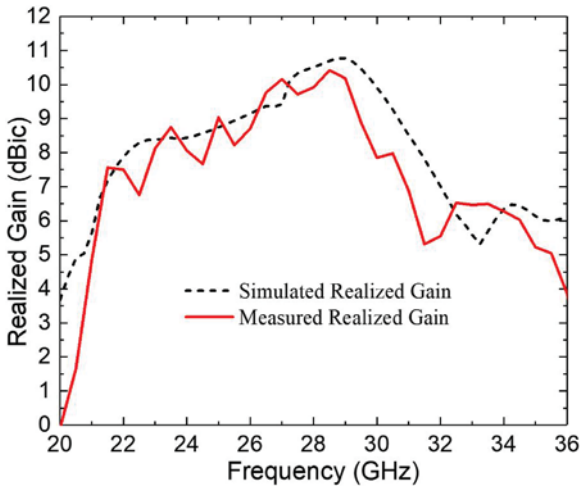

FIGURE 16 Simulated and measured realised gain of the proposed antenna.

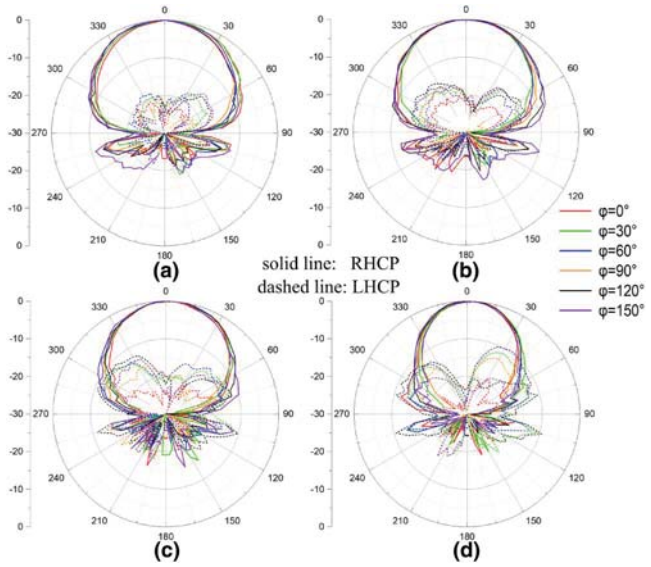

FIGURE 17 Measured normalised radiation patterns of the proposed antenna at four different frequency points. (a) 22 GHz, (b) 24 GHz, (c) 26 GHz, and (d) 28 GHz.

Rogers RO5880 substrate with a thickness of 1.57 mm. A 2.92 mm connector is applied to feed the antenna.

Figure 15 reveals the simulated and measured $|S_{11}|$s and ARs of the proposed antenna. The simulated AR and the impedance bandwidth of the proposed antenna are 48.71% (21.18–34.82 GHz) and 48.23% (21.32–34.87 GHz) respectively. The measured AR and the impedance bandwidth of the antenna are 51.3% (20–33.8 GHz) and 49.1% (21.2–35 GHz) respectively. As shown, the AR bandwidth overlaps well with the impedance bandwidth. The difference between the simulated and measured reflection coefficients mainly come from the manufacturing error of the diameter of the coaxial probe hole and the length of the coaxial probe pin. As shown in Figure 15, the whole AR curve moves slightly to the low

TABLE 2 Comparison of different wideband SIW CP antennas

Reference	Impedance bandwidth	Axial ratio bandwidth	Peak gain (dBic)	Size (λ^3)	Pattern symmetry	FBR (dB)
[1]	43% (24.1–37.3 GHz)	36.1% (26.1–37.6 GHz)	7.5 at 33 GHz	0.87 × 0.87 × 0.274	Asymmetrical	>14
[7]	40% (22–34 GHz)	30% (22–29.8 GHz)	7.8 at 29 GHz	3.78 × 2.87 × 1.23	Asymmetrical	N.G.
[10]	33.5% (20.1–28.2 GHz)	26.3% (20.3–26.45 GHz)	8.15 at 25 GHz	0.89 × 0.89 × 0.1	Asymmetrical	>14
[13]	31.5% (80.1–110 GHz)	34.7% (76–108 GHz)	9.6 at 106 GHz	2.84 × 2.53 × 0.2	Asymmetrical	>15
[17]	22.6% (37.5–47 GHz)	9.5% (40–44 GHz)	7.8 at 41.5 GHz	N.G.	Asymmetrical	>20
[19]	49.6% (36.2–60 GHz)	36.6% (39.8–57.6 GHz)	9.3 at 48 GHz	0.69 × 0.86 × 0.2	Asymmetrical	N.G.
[20]	27.1% (27.1–35.6 GHz)	16.3% (29.3–34.3 GHz)	9 at 34 GHz	0.93 × 0.93 × 0.13	Asymmetrical	>20
[25]	24.9% (51–65.5 GHz)	19.3% (54.4–66 GHz)	9.5 at 63 GHz	1.81 × 1.74 × 0.43	Asymmetrical	>10
[29]	51% (23.8–39.1 GHz)	48% (23.9–38.4 GHz)	8.6 at 38.7 GHz	0.80 × 0.80 × 0.25	Asymmetrical	>20
This work	49.1% (21.2–35 GHz)	51.3% (20–33.8 GHz)	10.42 at 28.5 GHz	0.82 × 0.82 × 0.21	Symmetrical	>20

Note: λ is the wavelength at the lowest frequency of the CP band.

Abbreviations: CP, circularly polarised; FBR, front-to-back ratio; SIW, substrate integrated waveguide.

frequency, which may be caused by fabrication and measurement errors of the proposed antenna.

As can be seen from Figure 16, the simulated and measured peak gain of the proposed antenna can reach 10.78 dBic at 29 GHz and 10.42 dBic at 28.5 GHz respectively. Figure 17 exhibits the measured radiation patterns of the proposed antenna at four different frequency points. This figure well confirms that the antenna has stable and symmetrical radiation patterns in different elevation planes over a wide frequency band (21–29 GHz). It is also noticed that the half-power beamwidth of the proposed antenna keeps nearly unchanged in different elevation planes. Moreover, the front-to-back ratio is >20 dB at all frequencies, which is another merit of the proposed antenna. In addition, the measured total efficiency of the proposed antenna is larger than 90% over the whole working band.

To demonstrate the merits of the presented antenna, Table 2 lists the comparison of different wideband SIW CP antennas. It is evident from the table, the proposed antenna can obtain wider impedance and AR bandwidth compared to other reported SIW CP antennas. In addition, the proposed antenna achieves the highest gain with a relatively compact size. Moreover, the proposed antenna shows great advantages in terms of the radiation pattern symmetry in different elevation planes. From this table, the superiority of the proposed antenna over other reported wideband SIW CP antennas can be observed, making it more advantageous for mm-wave applications.

4 | CONCLUSION

In this paper, a four PIFCs loaded mm-wave antenna has been presented. With the loaded parasitic components, great improvement on both the gain and bandwidth performance of the S-dipole antenna can be realised. Moreover, the radiation patterns can keep stable and highly symmetrical in different elevation planes over a wide operating band, which provides more uniform signal coverage than other mm-wave CP antennas. A prototype is fabricated and measured to validate the effectiveness of the design. With the merits of wide bandwidth, high gain, low profile, and highly symmetrical radiation patterns, the proposed antenna is promising for various mm-wave applications.

AUTHOR CONTRIBUTIONS

Xianting Xie: Methodology, Validation, Writing – original draft. **Long Zhang**: Conceptualisation, Supervision, Writing – review & editing. **Chunxu Mao**: Conceptualisation. **Yejun He**: Conceptualization. **Steven Gao**: Conceptualisation.

ACKNOWLEDGEMENT

This work was supported in part by the National Natural Science Foundation of China under Grants 61801299 and 62071306, in part by the Natural Science Foundation of Guangdong Province under Grant 2020A1515011037, and in part by the Shenzhen Science and Technology Program under Grants JCYJ20200109113601723, JSGG20210420091805014, and JSGG20210802154203011.

CONFLICT OF INTEREST

The author declares that there is no conflict of interest that could be perceived as prejudicing the impartiality of the research reported.

DATA AVAILABILITY STATEMENT

All the data in this manuscript is available.

ORCID

Xianting Xie https://orcid.org/0000-0003-3744-9066
Long Zhang https://orcid.org/0000-0003-0646-6699
Chunxu Mao https://orcid.org/0000-0002-4266-6826
Yejun He https://orcid.org/0000-0002-8564-5355
Steven Gao https://orcid.org/0000-0002-7402-9223

REFERENCES

1. Zhang, L., et al.: Wideband high-efficiency circularly polarized SIW-fed S-dipole array for millimeter-wave applications. IEEE Trans. Antenn.

Propag. 68(3), 2422–2427 (2020). https://doi.org/10.1109/tap.2019.2940468
2. Aziz, I., et al.: 28 GHz circular polarized fan-out antenna array with wide-angle beam-steering. Int. J. RF Microw. Computer-Aided Eng. 32(3), e23008 (2022). https://doi.org/10.1002/mmce.23008
3. Wang, L., Zhu, Z.: Broadband crossed dipole circularly polarized antenna with parasitic round-metal pillars. Int. J. RF Microw. Computer-Aided Eng. 31(9), e22786 (2021). https://doi.org/10.1002/mmce.22786
4. Yang, T., et al.: A low-profile circularly polarized antenna based on a circularly symmetric high impedance surface. Int. J. RF Microw. Computer-Aided Eng. 31(11), e22821 (2021). https://doi.org/10.1002/mmce.22821
5. Zhu, J., et al.: 60 GHz wideband high-gain circularly polarized antenna array with substrate integrated cavity excitation. IEEE Antenn. Wireless Propag. Lett. 17(5), 751–755 (2018). https://doi.org/10.1109/lawp.2018.2814051
6. Cheng, Y., Dong, Y.: Wideband circularly polarized planar antenna array for 5G millimeter-wave applications. IEEE Trans. Antenn. Propag. 69(5), 2615–2627 (2021). https://doi.org/10.1109/tap.2020.3028213
7. Zhang, Y., Jiao, Y., Zhang, L.: Wideband inhomogeneous-polarizer loaded circularly polarized SIW horn antenna for broadband millimeter-wave applications. IEEE Antenn. Wireless Propag. Lett. 18(7), 1448–1452 (2019). https://doi.org/10.1109/lawp.2019.2919636
8. Hesari, S.S., Bornemann, J.: Wideband circularly polarized substrate integrated waveguide endfire antenna system with high gain. IEEE Antenn. Wireless Propag. Lett. 16, 2262–2265 (2017). https://doi.org/10.1109/lawp.2017.2713720
9. Kumar, A., Srivastava, S.: Four element three-dimensional SIW horn antenna array for high-frequency applications. Int. J. RF Microw. Computer-Aided Eng. 31(6), e22660 (2021). https://doi.org/10.1002/mmce.22660
10. Yang, M., et al.: Wideband circularly polarized substrate-integrated embedded dielectric resonator antenna for millimeter-wave applications. IEEE Trans. Antenn. Propag. 68(2), 1145–1150 (2020). https://doi.org/10.1109/tap.2019.2938629
11. Akbari, M., et al.: Gain enhancement of circularly polarized dielectric resonator antenna based on FSS superstrate for MMW applications. IEEE Trans. Antenn. Propag. 64(12), 5542–5546 (2016). https://doi.org/10.1109/tap.2016.2623655
12. Yang, W., et al.: Design of a circularly polarized dielectric resonator antenna with wide bandwidth and low axial ratio values. IEEE Trans. Antenn. Propag. 67(3), 1963–1968 (2019). https://doi.org/10.1109/tap.2019.2891219
13. Cheng, X., et al.: Circularly polarized substrate-integrated waveguide tapered slot antenna for millimeter-wave applications. IEEE Antenn. Wireless Propag. Lett. 16, 2358–2361 (2017). https://doi.org/10.1109/lawp.2017.2718240
14. Han, W., et al.: Low-cost wideband and high-gain slotted cavity antenna using high-order modes for millimeter-wave application. IEEE Trans. Antenn. Propag. 63(11), 4624–4631 (2015). https://doi.org/10.1109/tap.2015.2473658
15. Xiao, J., et al.: High-gain and low-cost circularly polarized antenna array for 5G MMW applications. IET Microw., Antennas Propag. 16(2–3), 174–184 (2022). https://doi.org/10.1049/mia2.12230
16. Djerafi, T., et al.: Substrate integrated waveguide antenna subarray for broadband circularly polarised radiation. IET Microw. Antennas Propag. 8(14), 1179–1185 (2014). https://doi.org/10.1049/iet-map.2014.0121
17. Hu, J., et al.: Millimeter-wave wideband circularly polarized monopulse antenna using the sequential rotation feeding technique. Int. J. RF Microw. Computer-Aided Eng. 29(1), e21489 (2019). https://doi.org/10.1002/mmce.21489
18. Li, Y., Luk, K.: A 60-GHz wideband circularly polarized aperture-coupled magneto-electric dipole antenna array. IEEE Trans. Antenn. Propag. 64(4), 1325–1333 (2016). https://doi.org/10.1109/tap.2016.2537390
19. Tian, Y., et al.: Millimeter-wave wideband circularly polarized endfire planar magneto-electric dipole antenna based on substrate integrated waveguide. IEEE Antenn. Wireless Propag. Lett. 21(1), 49–53 (2022). https://doi.org/10.1109/LAWP.2021.3117311
20. Zhu, C., et al.: Low-profile wideband millimeter-wave circularly polarized antenna with hexagonal parasitic patches. IEEE Antenn. Wireless Propag. Lett. 20(9), 1651–1655 (2021). https://doi.org/10.1109/lawp.2021.3092139
21. Li, C., et al.: A metasurface-based multilayer wideband circularly polarized patch antenna array with a parallel feeding network for Q-band. IEEE Antenn. Wireless Propag. Lett. 18(6), 1208–1212 (2019). https://doi.org/10.1109/lawp.2019.2912624
22. Guntupalli, A.B., Wu, K.: 60-GHz circularly polarized antenna array made in low-cost fabrication process. IEEE Antenn. Wireless Propag. Lett. 13, 864–867 (2014). https://doi.org/10.1109/lawp.2014.2320906
23. Zuo, X., Yu, J.: Low-cost wide-bandwidth high-gain circularly polarized patch antenna array based on substrate integrated waveguide. Int. J. RF Microw. Computer-Aided Eng. 31(5), e22580 (2021). https://doi.org/10.1002/mmce.22580
24. Cao, B., Shi, Y., Feng, W.: W-band LTCC circularly polarized antenna array with mixed U-type substrate integrated waveguide and ridge gap waveguide feeding networks. IEEE Antenn. Wireless Propag. Lett. 18(11), 2399–2403 (2019). https://doi.org/10.1109/lawp.2019.2917774
25. Zhu, J., Liao, S., Li, S.: Circularly polarized 2-arm spiral antenna for 60-GHz applications. Microw. Opt. Technol. Lett. 59(12), 3119–3123 (2017). https://doi.org/10.1002/mop.30890
26. Fereidoony, F., Chamaani, S., Mirtaheri, S.A.: UWB monopole antenna with stable radiation pattern and low transient distortion. IEEE Antenn. Wireless Propag. Lett. 10, 302–305 (2011). https://doi.org/10.1109/lawp.2011.2141106
27. Eldek, A.A.: Ultrawideband double rhombus antenna with stable radiation patterns for phased array applications. IEEE Trans. Antenn. Propag. 55(1), 84–91 (2007). https://doi.org/10.1109/tap.2006.886560
28. Zhu, X., et al.: A dielectric-loaded dual-broadband printed dipole antenna with stable radiation pattern in the H-plane. IEEE Antenn. Wireless Propag. Lett. 18(9), 1761–1765 (2019)
29. Xie, X., et al.: Parasitic elements loaded MM-wave S-dipole antenna with wide bandwidth and high gain. In: 2021 International Conference on Microwave and Millimeter Wave Technology (ICMMT), pp. 1–3 (2021)

How to cite this article: Xie, X., et al.: High-gain wideband circularly polarised mm-wave antenna with highly symmetrical radiation patterns. IET Microw. Antennas Propag. 16(15), 911–918 (2022). https://doi.org/10.1049/mia2.12305